

# Force-Induced Bidirectional Stepping of Cytoplasmic Dynein

Arne Gennerich,<sup>1</sup> Andrew P. Carter,<sup>1</sup> Samara L. Reck-Peterson,<sup>1</sup> and Ronald D. Vale<sup>1,\*</sup>

<sup>1</sup>The Howard Hughes Medical Institute and the Department of Cellular and Molecular Pharmacology, University of California San Francisco, San Francisco, CA 94158-2200, USA

\*Correspondence: vale@cmp.ucsf.edu

DOI 10.1016/j.cell.2007.10.016

## SUMMARY

Cytoplasmic dynein is a minus-end-directed microtubule motor whose mechanism of movement remains poorly understood. Here, we use optical tweezers to examine the force-dependent stepping behavior of yeast cytoplasmic dynein. We find that dynein primarily advances in 8 nm increments but takes other sized steps (4–24 nm) as well. An opposing force induces more frequent backward stepping by dynein, and the motor walks backward toward the microtubule plus end at loads above its stall force of 7 pN. Remarkably, in the absence of ATP, dynein steps processively along microtubules under an external load, with less force required for minus-end- than for plus-end-directed movement. This nucleotide-independent walking reveals that force alone can drive repetitive microtubule detachment-attachment cycles of dynein's motor domains. These results suggest a model for how dynein's two motor domains coordinate their activities during normal processive motility and provide new clues for understanding dynein-based motility in living cells.

## INTRODUCTION

Cytoplasmic dynein is a two-headed molecular motor found in eukaryotic cells that uses the energy from ATP binding and hydrolysis to move toward the minus ends of microtubules. Cytoplasmic dynein, which is involved in a variety of motile processes such as mitotic spindle formation and the directed transport of organelles and mRNA (Vallee et al., 2004), is composed of two identical ~500 kDa heavy chains and several associated chains (Vale, 2003; Höök and Vallee, 2006). The heavy chain contains 6 AAA+ domains (AAA: ATPase associated with diverse cellular activities) arranged in a ring (Ogura and Wilkinson, 2001; Asai and Koonce, 2001) (Figure 1A). The first four AAA+ modules (AAA1–AAA4) have conserved nucleotide-binding and hydrolysis motifs. AAA domain 1 is essential for dynein motility, while the other sites (particular

AAA3) may contribute important regulatory functions (Silvanovich et al., 2003; Reck-Peterson and Vale, 2004; Takahashi et al., 2004; Kon et al., 2004, 2005).

The microtubule-binding and putative mechanical domains of dynein are distinctly different from those of kinesin and myosin. A small, globular microtubule-binding domain (MTBD) is poised at the tip of an ~10–15 nm long “stalk” (Asai and Koonce, 2001; Burgess et al., 2003) (Figure 1A), which is an antiparallel coiled-coil that lies between the fourth and fifth AAA domains (Gee et al., 1997; Koonce and Tikhonenko, 2000). A second appendage emerging from the ring is an ~10 nm long “linker” element that lies predominantly on top of the ring (Figure 1A), although it has been observed in a detached state (Burgess et al., 2003). The linker's position shifts relative to the AAA+ ring in different nucleotide states (Burgess et al., 2003; Kon et al., 2005), and this conformational change has been suggested to produce force and unidirectional motion. N-terminal to the linker is a dimerization domain that joins the two motor domains, although its structure and mechanism of dimerization are not known. The dimerization domain then extends into a “tail” region that binds several dynein-associated chains, which are involved in cargo binding (Vallee et al., 2004).

Recent single-molecule motility assays with purified mammalian dynein (Wang et al., 1995; King and Schroer, 2000; Mallik et al., 2004, 2005; Toba et al., 2006; Ross et al., 2006) and recombinant cytoplasmic dynein from yeast (Reck-Peterson et al., 2006) have begun to shed light on dynein's molecular mechanism. All of these studies have concluded that a single dimeric cytoplasmic dynein molecule can move processively along microtubules. However, the details of the stepping mechanism have been more controversial. Mallik et al. (2004) first reported that brain cytoplasmic dynein takes predominantly 24–32 nm steps along microtubules under no load but decreases its step size to 8 nm near its stall force of ~1 pN. In contrast, a more recent optical trapping study with brain dynein reports that cytoplasmic dynein takes load-invariant steps of 8 nm and stalls at 6–8 pN (Toba et al., 2006). Using single-molecule fluorescence microscopy, Reck-Peterson et al. (2006) observed predominantly 8 nm steps but also a wide range of larger (12–24 nm) steps and backward steps as well. Differing from the studies above, Ross et al. (2006) reported that dynein, in the presence of dynactin, can undergo long (>1000 nm) movements

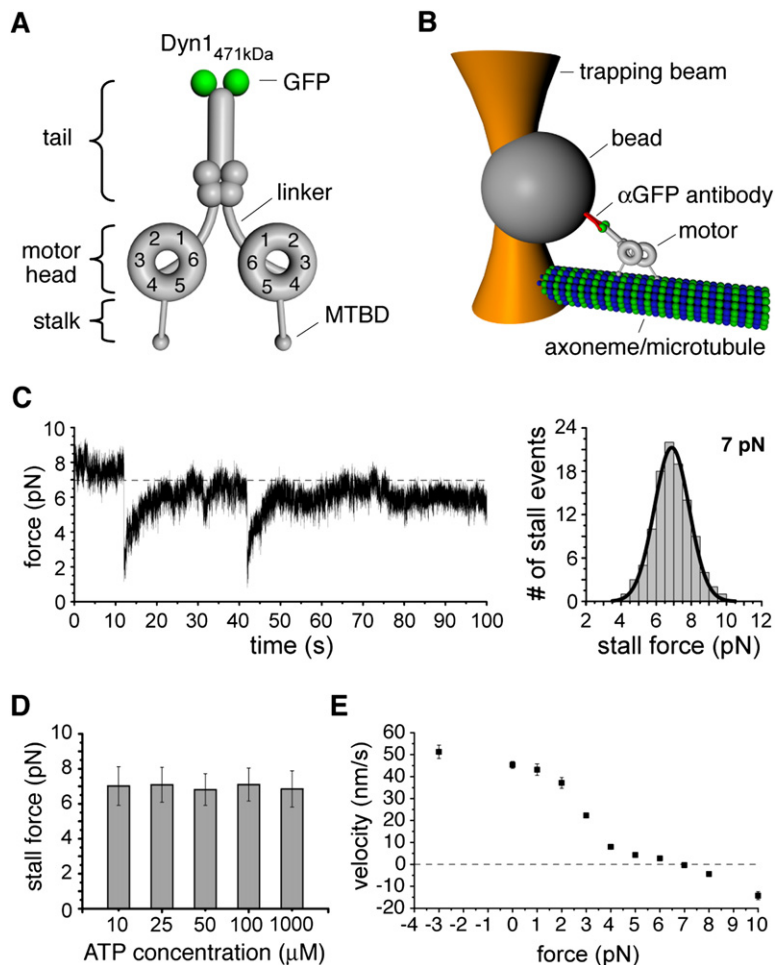


**Figure 1. Force Production by Full-Length Dynein**

(A) Illustration of the dynein dimer with associated chains and N-terminal GFPs.

(B) Schematic representation of the optical trapping assay (not to scale).

(C) Displacement of a single dynein molecule at 1 mM ATP in a fixed (nonfeedback) optical trap showing successive motor detachments and stalling events (trap stiffness:  $k = 0.055$  pN/nm). The inset on the right side shows the stall force distribution ( $6.9$  pN  $\pm$  1 pN; mean  $\pm$  SD;  $n = 108$ ).

(D) Stall force as a function of ATP concentration. Values are displayed as mean  $\pm$  SD ( $n = 20$ –108).

(E) Velocity-force relationship at 1 mM ATP. All velocities were measured with the optical trap maintaining a constant load using feedback control, except the zero load velocity, which was measured by tracking the GFP-tagged motors in a single-molecule fluorescence assay. Values are displayed as mean  $\pm$  SEM ( $n = 35$ –151).

toward the plus as well as the minus ends of microtubules. Thus, the mechanism of cytoplasmic dynein stepping and force production remains controversial.

In order to dissect the dynein mechanism, we used a force-feedback optical trap to analyze the stepping behavior of native and artificially dimerized yeast cytoplasmic dynein as a function of load. At low loads (1 pN), we show that dynein primarily advances by 8 nm as well as occasionally larger (12–24 nm) increments. Increasing loads (3–6 pN) frequently induce large (12–24 nm) alternating forward-backward displacements that fail to advance the motor and might be caused by a force-induced conformational change in the positioning of the two motor domains in the dynein dimer. Strikingly, we also find that dynein will walk processively toward either the minus or plus ends of microtubules under an applied force in the absence of nucleotide hydrolysis, a behavior that distinguishes dynein from kinesin-1 and myosin-V. A small assisting force ( $-3$  pN) causes dynein to step toward the microtubule minus end (its normal direction) in the absence of nucleotide, while a much larger force (7–10 pN) is required to induce dynein stepping toward the plus end. The directional asymmetry of this force-induced, nucleotide-independent stepping suggests a model for how

dynein's two motor domains are coordinated during normal processive motility and provides new clues for how dynein might respond to antagonistic forces in living cells.

## RESULTS

### Stall Force of Full-Length Yeast Cytoplasmic Dynein and Reversed Motion at Superstall Loads

Our previous study (Reck-Peterson et al., 2006) showed that *S. cerevisiae* full-length cytoplasmic dynein (Dyn1<sub>471kDa</sub>, herein referred to as “dynein”), a complex of the dimerized motor-containing heavy chain and several associated chains, is a highly processive motor. Here we coupled dynein to anti-GFP antibody-coated 1  $\mu$ m latex beads through an N-terminal GFP-tag on the motor tail (Figures 1A and 1B); the dynein density on the beads was adjusted so that there was a >99% probability that bead movements were due to single dynein molecules (Supplemental Data and Figure S1). Dynein-coated beads captured in a fixed position optical trap (nonfeedback mode) moved along sea urchin axonemes away from the trap center until they eventually stalled at an average rearward load of  $\sim 7$  pN (Figure 1C), similar to the stall force of kinesin-1 (Visscher et al., 1999). Remarkably,

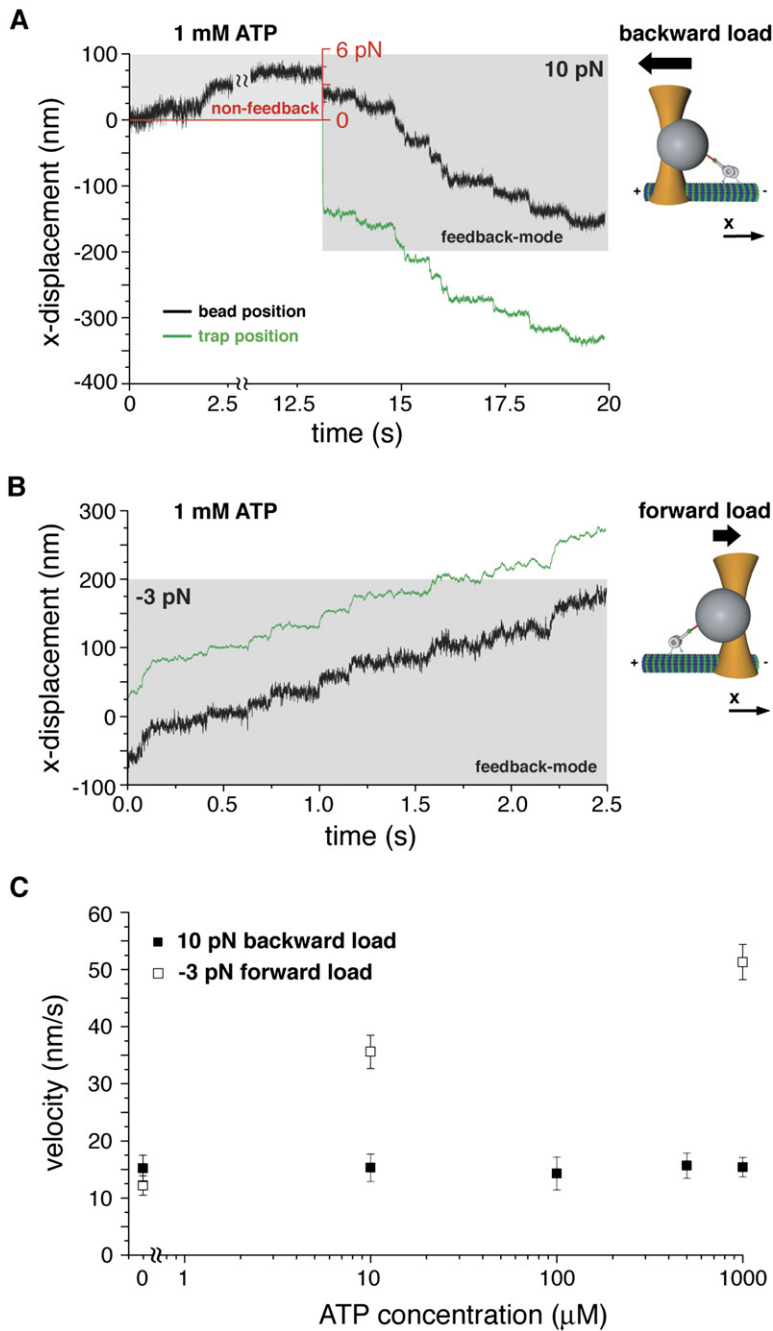


**Figure 2. Forced-Backward and Assisted-Forward Movement of Full-Length Dynein in the Presence of ATP Hydrolysis**

(A) Optical trapping record of forced-backward movement of Dyn1<sub>471kDa</sub> under 10 pN super-stall force (force-feedback mode, gray-shaded area) following a motor run under increasing rearward load (nonfeedback, upper corner left, the red coordinate system indicates the corresponding force) in the presence of 1 mM ATP (trap stiffness:  $k = 0.056$  pN/nm). (B) Forward movement of Dyn1<sub>471kDa</sub> under a  $-3$  pN assisting load and 1 mM ATP (trap stiffness:  $k = 0.033$  pN/nm). (C) Velocity (absolute values) of Dyn1<sub>471kDa</sub> movement at 10 pN rearward load ( $n = 54-77$ ) and  $-3$  pN forward load ( $n = 52-60$ ), respectively, as a function of ATP concentration. Values are displayed as mean  $\pm$  SEM.

and in contrast to kinesin under similar salt conditions (Figure S2A), a stalled dynein molecule remained tenaciously bound to a microtubule, often for several minutes, before dissociating (Figure 1C). The stall force of dynein was unchanged when the ATP concentration was decreased from 1 mM to 10  $\mu$ M (Figure 1D), in contrast to an earlier report on brain cytoplasmic dynein (Mallik et al., 2004) but in agreement with Toba et al. (2006).

We next examined whether dynein would walk backward (toward the microtubule plus end) when the applied load exceeded the stall force, as has been described for

kinesin-1 and myosin-V (Carter and Cross, 2005; Gebhardt et al., 2006). To perform this experiment, we applied a constant 10 pN load to the motor using the force-feedback mode of the optical trap (Supplemental Data). When this superstall force was applied in the presence of 1 mM ATP, single dynein molecules moved processively backward toward the microtubule plus end with an average speed of  $\sim 15$  nm/s (Figures 2A, 2C, and S3). We next tested whether an assisting force (negative force value) directed toward the microtubule minus end could accelerate dynein movement (Figure 2B). However, the

average dynein velocity under a  $-3$  pN assisting load (51 nm/s) was comparable to that observed under unloaded conditions (45 nm/s) (Figures 1E and 2C). By applying different constant forces, we were able to generate a force-velocity curve for dynein spanning between  $-3$  pN and 10 pN force load (Figure 1E).

### Force-Induced, Bidirectional Dynein Movement in the Absence of ATP Hydrolysis

To better understand how external forces affect dynein movement, we studied the ATP dependence of movement under an assisting ( $-3$  pN) and superstall (10 pN) force. Remarkably, the velocity of plus-end-directed motion under a superstall load did not depend upon ATP concentration ( $\sim 15$  nm/s over a wide range of ATP concentrations; Figure 2C). Even in the absence of ATP (ATP/ADP depleted by the enzyme apyrase), a 10 pN rearward pull caused dynein to move processively toward the microtubule plus end (Figures 3A and S4A). In contrast, the velocity of minus-end-directed movement under a  $-3$  pN assisting force was ATP dependent, decreasing by  $\sim 30\%$  at 10  $\mu$ M ATP (Figure 2C). However, surprisingly, minus-end-directed motion ( $\sim 12$  nm/s) persisted under nucleotide-free conditions with an applied  $-3$  pN assisting load (Figure 3B).

We next examined the force dependence of nucleotide-independent dynein motility. Without an applied load, all dynein-coated beads that bound to a microtubule (105 beads) did not move, confirming complete nucleotide depletion by apyrase (Supplemental Data). In contrast, with a rearward 10 pN force,  $\sim 90\%$  of the dynein-coated beads that bound to the microtubule exhibited plus-end-directed motion within an  $\sim 10$  s window of applied load (56 out of 62). At 7 pN (the stall force), fewer beads (13 out of 25) moved in a similar period of applied force; for beads that failed to move, increasing the load from 7 to 10 pN frequently induced movement (Figure 3A, lower inset). The subset of dynein-coated beads that moved at 7 pN also advanced at a slower velocity ( $-6.7 \pm 1.5$  nm/s, mean  $\pm$  SEM) compared with those that moved at 10 pN ( $-15.2 \pm 2.3$  nm/s). At a lower load of 3 pN, only 1 out of 24 beads that bound to the microtubule moved within a 10 s window of applied load. In contrast, with an assisting (minus-end-directed) load of  $-3$  pN, the majority of dynein beads that bound to a microtubule exhibited continuous movement (79 out of 83 beads) (Figures 3B and S4C). Thus, nucleotide-independent movement of dynein is force dependent and much lower forces are necessary to induce movement toward the microtubule minus end than toward the plus end.

We next wished to establish that the force-induced, nucleotide-independent movement was due to dynein stepping, as opposed to detachment of both motor heads, motion along the microtubule axis due to the pull of the optical trap, and then reattachment to the microtubule track (referred to here as “slippage”). To test whether slippage might be occurring, we applied a simultaneous lateral and backward load (9 pN perpendicular and 10 pN parallel to

the microtubule axis; Figure 3C). If the dynein motor completely detached from the microtubule, the lateral load would pull the bead away from the axoneme, which should terminate a dynein run (Figure S4B; Gebhardt et al., 2006). However, dynein displayed long processive runs toward the microtubule plus end under such conditions (Figure 3C). Nucleotide-independent dynein movement under forward and backward loads also occurred in small, discrete steps that were similar in size to those observed in the presence of ATP (predominantly  $\sim 8$  nm; see next section) (Figure 3D). Large steps that exceeded the maximum step size observed under simultaneous lateral and longitudinal forces ( $\sim 30$  nm; Figure S4B) and at zero load ( $\sim 32$  nm; Reck-Peterson et al., 2006) occasionally were observed under 10 pN backward load and might be attributable to slippage, but they constituted a very small fraction of the total steps scored ( $\sim 2\%$ ; Figure 3D).

In summary, force alone can induce bidirectional dynein stepping in the absence of nucleotide hydrolysis, with a clear asymmetry in the plus- and minus-end directions along the microtubule axis. This behavior distinguishes dynein from kinesin-1 (which has been suggested to require ATP for force-induced backward as well as forward stepping; Carter and Cross, 2005) and myosin-V (which will step backward without ATP hydrolysis but not forward; Gebhardt et al., 2006).

### Load-Dependent Stepping Behavior of Cytoplasmic Dynein in the Presence of ATP

To gain additional mechanistic insight into cytoplasmic dynein motility, we analyzed the stepping behavior of single dynein molecules under different constant loads with the force-feedback optical trap in the presence of 1 mM ATP. The displacement traces displayed considerable noise due to thermal fluctuations of the bead-dynein complex (Figure 4). To identify steps with minimal bias, we used a step finding algorithm (Kerssemakers et al., 2006) and verified the ability of this algorithm to detect artificial steps embedded in noise similar to those observed in dynein optical trapping records (Supplemental Data).

One clear feature of the dynein displacement traces is the presence of both forward as well as backward steps at all loads tested (Figure 4; see Figures S5–S7 for additional traces). At the lowest load of 1 pN, dynein predominantly stepped toward the minus end, although  $\sim 30\%$  of the measured steps were in the reverse direction (Figure 4A). This percentage of backward steps is slightly higher than that measured at zero load ( $\sim 20\%$ ; Reck-Peterson et al., 2006). Thus, even at loads below the stall force, dynein has a relatively weak directional bias. In contrast, using the same optical trap, we rarely observed backward kinesin steps, even at loads approaching stall (Figure S2B). At the stall force of 7 pN, dynein stepping continued, but the numbers of backward and forward steps were approximately equal (Figure S8D), resulting in little or no net movement (Figures 1C and 1E). At the superstall force of 10 pN,  $\sim 75\%$  and  $\sim 25\%$  of the steps were directed toward the microtubule plus and minus

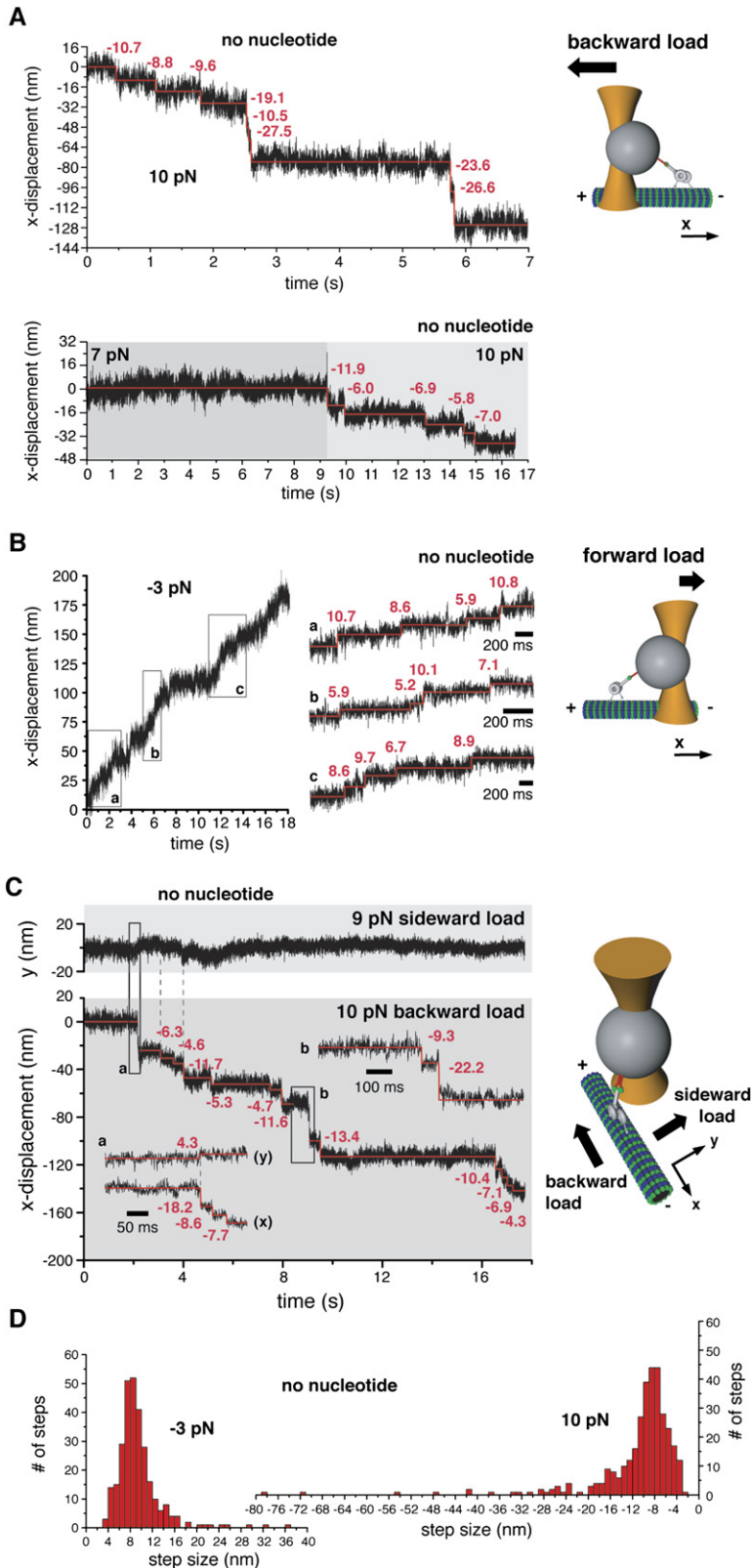


**Figure 3. Forced-Backward and Forced-Forward Movement of Full-Length Dynein in the Absence of ATP Hydrolysis**

(A) Stepwise backward movement of Dyn1<sub>471kDa</sub> under 10 pN superstall force in the absence of ATP (trap stiffness:  $k = 0.055$  pN/nm) (upper inset). The lower inset shows an example record of a microtubule-bound Dyn1<sub>471kDa</sub> motor under stall and superstall loads in the absence of ATP. The motor is tightly bound in rigor for  $\sim 9$  s under 7 pN stall force without detectable advancing steps and starts to step backward after the application of a 10 pN superstall force (trap stiffness:  $k = 0.063$  pN/nm). The raw data are shown in black and the steps detected by the step-finding program in red.

(B) Optical trapping record of microtubule minus-end-directed movement of Dyn1<sub>471kDa</sub> under  $-3$  pN forward load in the absence of ATP (trap stiffness:  $k = 0.055$  pN/nm). The trace segments (a, b and c) correspond to the trace sections indicated by the rectangular boxes.

(C) Forced-backward movement of Dyn1<sub>471kDa</sub> under a simultaneous lateral load of 9 pN and a longitudinal backward load of 10 pN (trap stiffness:  $k = 0.07$  pN/nm). The record shows the displacements of the trapped bead along the microtubule axis ( $x$ ) and in perpendicular direction ( $y$ ). The inserted trace segments (a and b) correspond to the trace sections indicated by the rectangular boxes.

(D) Histograms of step sizes for microtubule-minus-end-directed movement under  $-3$  pN assisting load (left,  $n = 292$ ) and microtubule-plus-end-directed movement under 10 pN rearward load (right,  $n = 332$ ) in the absence of nucleotide.

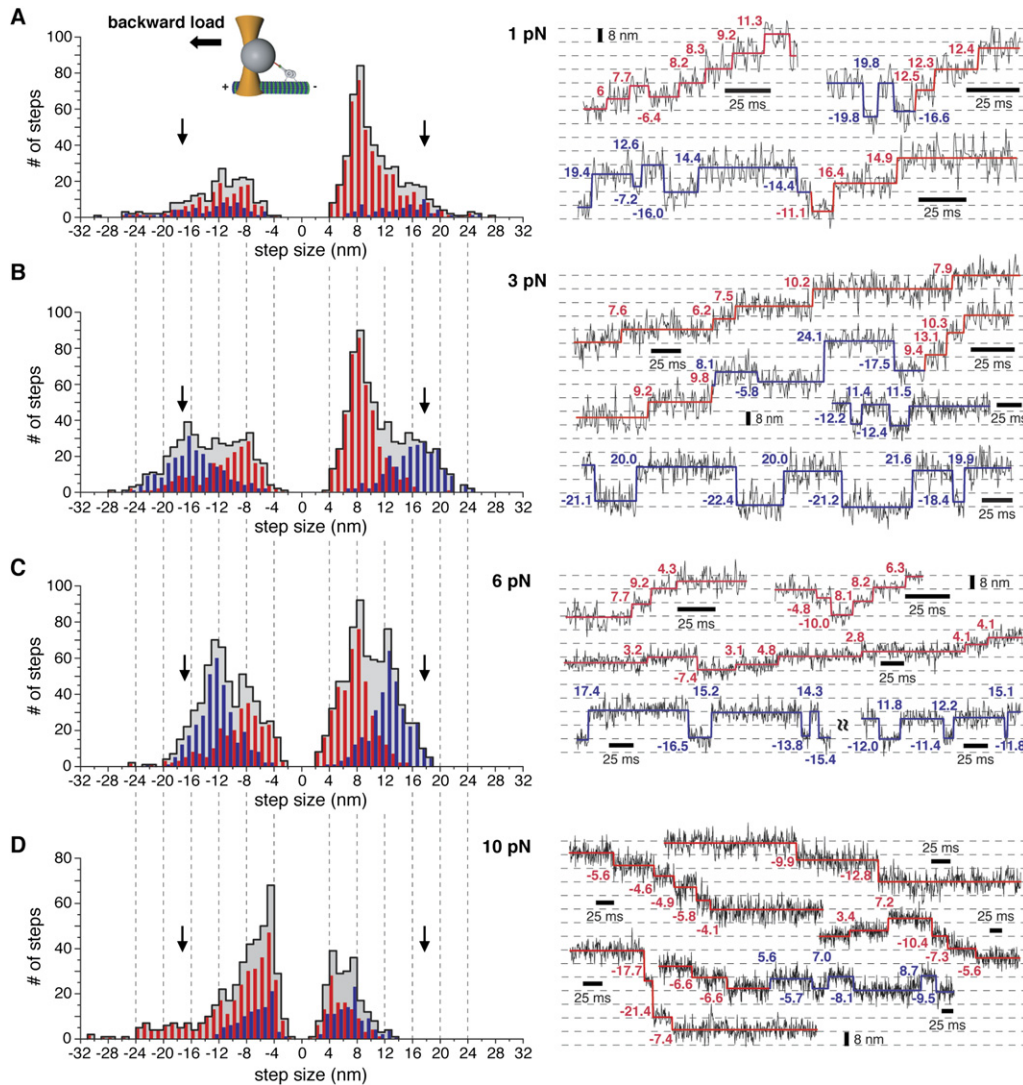


**Figure 4. Load-Dependent Stepping Behavior of Full-Length Dynein in the Presence of ATP**

(A–D) Histograms of steps sizes and example trace segments measured under 1 pN ( $n = 716$ ), 3 pN ( $n = 1104$ ), 6 pN ( $n = 1314$ ), and 10 pN ( $n = 642$ ) constant rearward load (force-feedback). The gray-shaded histograms correspond to the combined step size data and the red and blue histogram bars indicate the steps assigned to the advancing and nonadvancing modes, respectively. The raw stepping data are shown in black and the steps detected by the step-finding program in red (advancing mode) and blue (nonadvancing mode). The probability  $p_b^{\text{adv}}$  for taking a backward step in the advancing mode ( $p_f^{\text{adv}} + p_b^{\text{adv}} = 1$ , with  $p_f^{\text{adv}}$  being the probability for taking a forward step in the advancing mode) at 1, 3, 6, and 10 pN load is 0.26, 0.34, 0.4, and 0.75, respectively (calculated from advancing step size histograms shown in red). The probability  $p^{\text{non-adv}}$  for taking any step in the non-advancing mode ( $p^{\text{adv}} + p^{\text{non-adv}} = 1$ , with  $p^{\text{adv}}$  being the probability for taking any step in the advancing mode) is 0.19, 0.42, 0.5, and 0.31 at 1, 3, 6, and 10 pN, respectively.

ends, respectively (Figure 4D). The minus-end-directed steps at the 10 pN load are driven by ATP turnover since they are not observed under nucleotide-free conditions (Figure 3D).

Our step size histograms also revealed that dynein takes variable sized steps and that load affects the step size distributions (Figure 4, gray-shaded histograms). At 1–3 pN rearward load at 1 mM ATP, the major peak of minus-end-directed steps was centered at 8 nm with a broad shoulder of larger steps (12–24 nm). These large

steps are not due to rapid multiple ATP-driven 8 nm steps in succession since the same step size distribution was observed when the motor speed was decreased by lowering the ATP concentration to 10  $\mu\text{M}$  (Figure S9). The peak of backward steps at this load was centered between 8 and 12 nm. This overall distribution is similar to the step size distribution obtained at zero load (Reck-Peterson et al., 2006). At very high loads of 6–10 pN, we observed increased numbers of  $\sim 4$  nm steps, which were distinguishable from the noise at this high load (Figure 4C,

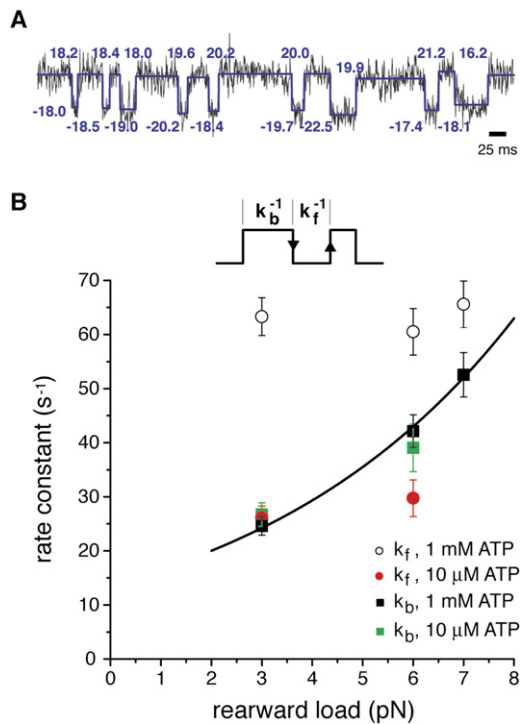


**Figure 5. Kinetics of Nonadvancing Stepping of Full-Length Dynein and Load Dependence of Backward Steps**

(A) Example record of nonadvancing stepping under 3 pN rearward load.

(B) Rate constants  $k_f$  and  $k_b$  of nonadvancing forward and backward stepping as a function of load and ATP concentration. The rate constants (mean values) were obtained by cumulative-distribution analysis of the underlying dwell time data (Figure S12). The load dependence of the rate constant  $k_b$  at 1 mM ATP (black squares) can be expressed by an exponential function of the form  $k_b^0 \exp(Fd/k_B T)$ , with  $k_b^0 = 13.7 \pm 1.0 \text{ s}^{-1}$  and  $d = 0.79 \pm 0.05 \text{ nm}$ . Error estimates were calculated as the SD of fit parameters derived from 200 bootstrap samples drawn from the underlying data set.

middle trace and Figure S7). We also observed an appearance of large (12–20 nm) steps in both the forward (minus end) and backward (plus end) direction at intermediate loads of 3–6 pN (Figures 4B and 4C). Further characterization of these large, load-induced steps is described in the next section.

### A Nonadvancing Mode of Dynein Stepping Induced by High Loads

An increase in larger steps at higher loads was not anticipated, especially as one prior study reported that the step size of dynein decreases with load (Mallik et al., 2004). Inspection of dynein displacement traces at 3 and 6 pN load revealed that large steps often were contained in long stretches of repeating forward-backward steps that resulted in little or no net displacement of the motor (Figures 4B, 4C, 5A, and S6–S10). Such repetitious forward-backward stepping was uncommon at 1 pN load, where dynein generally took forward steps, interspersed

with a single or a few successive (<3) backward steps (Figures 4A and S5).

To examine the characteristics of forward-backward stepping quantitatively, we classified dynein stepping into two categories: an “advancing mode” characterized by two or more successive steps in the same direction (toward either the microtubule minus end or plus end with one intervening reverse step allowed [red lines and histogram bars in Figure 4]), and a “nonadvancing mode” characterized by two or more successive forward-backward steps (blue lines and histogram bars in Figure 4) (see Supplemental Experimental Procedures for more details on classification and statistical analysis). In other words, clustered forward-backward steps are classified as “nonadvancing” while all other stepping is considered to be “advancing.” This classification, while perhaps somewhat arbitrary, revealed very different properties for the advancing and nonadvancing modes of dynein stepping. The advancing mode predominated at low loads (1 pN); the step size distribution was centered at 8 nm (with a shoulder at 12 nm) and decreased to 4–8 nm at 6 pN (Figure 4). Interestingly, when load approached the stall force, ~4 nm steps constituted the major peak in the histogram at 7 and 10 pN load (Figures 4D and S8D). These observations indicate that dynein mostly takes small advancing steps and the entire step size distribution shows a modest shift toward smaller size steps with increasing load.

Analysis of the nonadvancing steps revealed several distinct properties from the advancing steps. First, the proportion of nonadvancing steps increased dramatically with load (compare red and blue histograms at 1 and 3 pN in Figure 4). Nonadvancing steps were also larger than advancing steps and accounted for the majority of the 16–20 nm steps at 3 pN. Thus, nonadvancing mode accounts for the unexpected increase in larger steps in the histogram at 3 pN load (Figure 4B). The size of the nonadvancing steps also was affected by load as their distribution shifted to primarily 12–16 nm at 6 pN (Figure 4C). We also observed several nonrandom patterns of nonadvancing stepping (Figure S11). First, a nonadvancing backward step tended to be of the same size as the preceding forward step (at a significantly higher probability than one would expect from the total step size distribution; Figure S11B), suggesting that a large nonadvancing backward step is likely the reversal of a process that led to the forward step. Large forward-backward steps of the same size also tended to cluster together (Figures S11C and S11D), thus returning the bead repeatedly to the same forward and backward positions (see nonadvancing trace segments in Figures 4B, 4C and 5A). The clustering of large similarly sized forward-backward steps also occurred more frequently than statistically expected (Figures S11C and S11D). An interpretation of this nonrandom behavior is that these discrete step sizes reflect particular structural states of the dynein motor that can persist for several ATPase cycles (see Discussion). In contrast, 8 nm forward-backward steps under 3 and 6 pN load did not occur more often than statistically expected (Figures S11C and

S11D). Collectively, these results support the notion that the nonadvancing mode (characterized by large consecutive forward-backward steps) constitutes a distinct pathway from the advancing mode (characterized by mostly 8 nm forward steps; Figure 4).

To gain further insight into dynein's nonadvancing stepping behavior (Figure 5A), we analyzed how load and ATP concentration affect the rates of forward ( $k_f$ ) and backward ( $k_b$ ) steps in this nonadvancing mode. The rate constants were obtained by analyzing the dwell times between a forward to a backward step or between a backward to a forward step (Figures 5B and S12). The analysis revealed that  $k_b$  increased with increasing load (Figure 5B, black squares), while  $k_f$  was relatively unaffected by load (Figure 5B, open circles). The effect of force on  $k_b$  can be expressed by a single exponential function of the form  $k_b^0 \exp(Fd/k_B T)$ , where  $k_b^0$  is the rate constant in the absence of load,  $d$  is the transition-state distance along the direction of applied load from the ground state to the transition state,  $k_B$  the Boltzmann constant, and  $T$  the absolute temperature (Bell, 1978), which yields the parameters  $k_b^0 = 13.7 \pm 1.0 \text{ s}^{-1}$  and  $d = 0.79 \pm 0.05 \text{ nm}$ . The measured transition-state distance is similar to the distance measured for the force-induced unbinding of the myosin-V lead head (0.6 nm, Gebhardt et al., 2006). In contrast, reducing the ATP concentration to  $10 \mu\text{M}$  (a value close to  $K_m$ , Figure S9) did not significantly affect  $k_b$  (Figure 5B, green squares) but decreased  $k_f$  by two-fold (Figure 5B, red circles). In summary, the rate of nonadvancing backward stepping is increased by load but unaffected by ATP, while the rate of nonadvancing forward stepping is unaffected by load and dependent on ATP. These results suggest that the forward step is driven by an ATP-dependent advancement of one of the dynein heads (most likely the trailing head past the leading head), while the backward step represents a detachment of the leading dynein head followed by its reattachment to a rearward binding site.

### Role of Dynein's Linker Element in Force Production and Stepping

We next wanted to examine the structural basis of the large dynein steps, which are particularly prevalent in the nonadvancing mode. One model proposed is that large steps may arise when the two dynein motor domains separate into an "extended" conformation (Figure 6A) (Reck-Peterson et al., 2006). Indeed, the large (12–24 nm) nonadvancing forward-backward steps observed at higher loads (3–7 pN) might be due to separation of the dynein heads caused by a mechanical force. According to this model, the maximum head-to-head separation and reach of the dynein dimer in its extended conformation is likely limited by the length of the linker elements interconnecting the dynein heads to the dimerization domain. To test this idea, we examined the stepping behavior of two tail-truncated dynein motors (GST-Dyn1<sub>314kDa</sub> and GST-Dyn1<sub>331kDa</sub>) that are artificially dimerized by an N-terminal fusion to glutathione S-transferase (GST) (Figure 6B)

(Reck-Peterson et al., 2006). In the shorter construct (GST-Dyn1<sub>314kDa</sub>), the distance between the motor heads is likely reduced compared to full-length dynein and the longer construct GST-Dyn1<sub>331kDa</sub>. Both GST-Dyn1<sub>314kDa</sub> and GST-Dyn1<sub>331kDa</sub> were previously shown to be processive in a single-molecule TIRF assay, having similar velocities and run lengths to the full-length dynein (Reck-Peterson et al., 2006). GST-Dyn1<sub>314kDa</sub> is the shortest construct that allows dynein motility; a further 26 aa truncation produced a motor that cannot move and has greatly impaired ATPase activity.

GST-Dyn1<sub>331kDa</sub> moved in the optical trap and stalled at a rearward load of 4.8 pN (Figure 6C), which is reduced compared to full-length dynein (6.9 pN,  $p < 0.001$ , two-sided Student's *t* test). GST-Dyn1<sub>331kDa</sub> also exhibited a nonadvancing stepping mode, with the distributions of forward-backward steps centered at  $\sim 16$ – $20 \text{ nm}$  (Figures 6C and S13). The additional 145 aa truncation of dynein's proximal tail to create GST-Dyn1<sub>314kDa</sub> further reduced the maximal force production (stall force of 4.0 pN, Figure 6D), the percentage of nonadvancing forward-backward stepping at 3 pN, and the number of overall steps that were  $>12 \text{ nm}$  (Figures 6D and S14). These differences between the two truncated dynein constructs suggest that reducing the spacing between the dynein heads limits the ability of the motor to take longer steps and produce greater force. The tail truncation in GST-Dyn1<sub>314kDa</sub>, however, did not interfere with force-induced ATP-independent movements toward either the microtubule minus end or plus end (Figure S14). Interestingly, the velocities of nucleotide-independent movement and the forces needed to induce such movement were similar for GST-Dyn1<sub>314kDa</sub> and full-length dynein (see legend to Figure S14), suggesting that the two motors have similar microtubule-binding affinities in the nucleotide-free state.

If head-head spacing is an important determinant for force and step size, then it might be possible to restore these impaired activities in Dyn1<sub>314kDa</sub> by inserting an artificial linker between the head and beginning of the dimerization domain. We tested this idea by inserting an artificial linker ( $\alpha$ -actinin repeats 1 and 2) in between the N terminus of Dyn1<sub>314kDa</sub> and GST (Figure 6B). The  $\alpha$ -actinin insert has a length of  $\sim 12 \text{ nm}$  and is composed of two rigid, triple-helical bundles linked by an uninterrupted  $\alpha$  helix (Kliche et al., 2001). This motor, termed GST- $\alpha 2$ -Dyn1<sub>314kDa</sub>, was processive with a primary advancing step size of  $\sim 8 \text{ nm}$  (Figure 6E) and stalled at an average load of 5.2 pN (Figure 6E), which was significantly higher than the parent GST-Dyn1<sub>314kDa</sub> construct ( $p < 0.001$ ). Significantly, GST- $\alpha 2$ -Dyn1<sub>314kDa</sub> also displayed a significant number of  $>12 \text{ nm}$  forward-backward steps at 3 pN load in the nonadvancing stepping mode (Figures 6E and S15) compared to Dyn1<sub>314kDa</sub> (Figure 6D). Thus, GST- $\alpha 2$ -Dyn1<sub>314kDa</sub> appears to more closely resemble the stepping behavior of GST-Dyn1<sub>331kDa</sub>, indicating that the  $\alpha$ -actinin repeat sequence partially restored the function of the native dynein linkers that precede the dimerization domain.

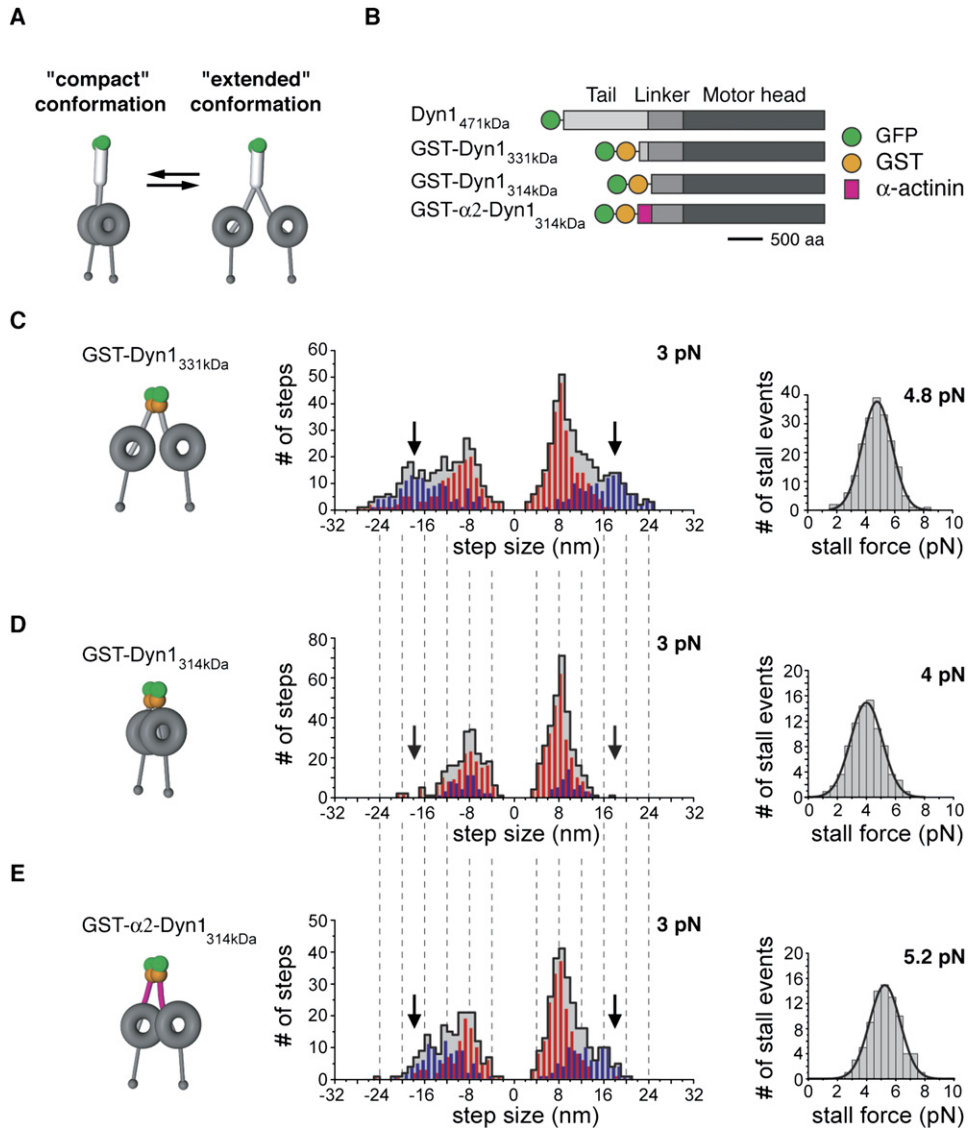


**Figure 6. Analysis of Truncated, Artificially Dimerized Dynein Motors in the Optical Trapping Assay and Illustration of the “Compact” and “Extended” Dynein Conformations**

(A) Compact and extended conformations of the dynein dimer may explain a wide variation in step size. In its compact state, the two dynein rings are restrained and located in close proximity and perhaps overlapping due to direct head-to-head “interactions” or a “zipping” of the proximal tail. The loss of physical interactions or an “unzipping” of the proximal tail might cause a less restrained extended conformation with an increased head-to-head distance.

(B) Diagram of constructs showing the dynein heavy chain truncations and tags.

(C) Force production and stepping behavior of GST-Dyn1<sub>331kDa</sub>. Left: Schematic of the GST-Dyn1<sub>331kDa</sub> motor. Center: Histograms of the combined step size data (gray-shaded), classified according to the advancing (red histogram bars) and nonadvancing modes (blue histogram bars) (3 pN force-feedback data, n = 670). Right: Stall force distribution of GST-Dyn1<sub>331kDa</sub> (4.8 pN ± 1.0 pN; mean ± SD; n = 195).

(D) Force production and stepping behavior of GST-Dyn1<sub>314kDa</sub>. Left: Schematic of the GST-Dyn1<sub>314kDa</sub> motor. Center: Histograms of the combined, advancing and non-advancing step size data (3 pN force-feedback data, n = 518). Right: Stall force distribution of GST-Dyn1<sub>314kDa</sub> (4.0 pN ± 1.1 pN; mean ± SD; n = 91).

(E) Force production and stepping behavior of the dynein construct GST-α2-Dyn1<sub>314kDa</sub> with artificial linker elements. Left: Schematic of the GST-α2-Dyn1<sub>314kDa</sub> motor. Center: Histograms of the combined, advancing, and nonadvancing step size data (3 pN force-feedback data, n = 457). Right: Stall force distribution of GST-α2-Dyn1<sub>314kDa</sub> (5.2 pN ± 1.1 pN; mean ± SD; n = 80).

## DISCUSSION

Our optical trapping experiments have revealed several force-dependent properties of dynein, which distinguish it from kinesin and myosin. Yeast dynein frequently remains bound to the microtubule for several minutes at stall loads, conditions that tend to dissociate other cytoskeletal motors from their tracks within a few seconds. We also show that dynein is a more irregular stepper (variable step size ranging from 4–24 nm) and its directionality is less robust than that of kinesin-1 and myosin-V. In addition, we demonstrate the unique finding that a mechanical load in the absence of ATP hydrolysis will cause dynein to step processively toward either the minus end or plus end of microtubules, depending upon the direction of the pull. However, there is a significant mechanical asymmetry in the dynein motor, as evidenced by the amount of force required to elicit movement and the ATP dependence of movement in the two directions. The implications of these findings for dynein's mechanism and its biological roles are discussed below.

### Models for the Variable Step Sizes and Load-Dependent Stepping of Dynein

The substantial step size variation of yeast cytoplasmic dynein shows similarities and differences with other cytoskeletal motor proteins. Kinesin-1, for example, takes regular 8 nm steps (Svoboda et al., 1993) and takes very few backward steps under substall loads. Myosin-V shows a slight variation in step size around the mean of 36 nm (31–41 nm) due to a diffusional component of the step that enables the leading head to bind to one of three available subunits on the actin filament (Walker et al., 2000; Mehta et al., 1999; Veigel et al., 2002). Dynein, on the other hand, takes a wide range of steps (4–24 nm) and a significant fraction of backward steps as well, which is more akin to the step size variation seen for myosin-VI (~21–51 nm; Rock et al., 2001; Nishikawa et al., 2002). In addition to the occasional backward steps interspersed among the forward steps, our study also demonstrates a previously undescribed nonadvancing forward-backward stepping mode of cytoplasmic dynein at 3–7 pN load. Such repeated forward-backward stepping well below the stall force level is not observed for myosin-V, myosin-VI, or kinesin-1 (Veigel et al., 2002; Rock et al., 2001; Carter and Cross, 2005). It remains possible that this nonadvancing stepping might be a unique feature of yeast cytoplasmic dynein, which could have an increased probability for a transition into the forward-backward stepping mode due to its slower velocity and its lower dissociation rate from the microtubule under load compared with dyneins from other species.

Dynein's variation in step size and nonadvancing stepping at higher loads might be explained by a general structural model in which the motor dimer can adopt either a "compact" or "extended" conformation (Figure 6A). In the "compact" state, the two dynein rings are located in close proximity, perhaps even overlapping, which

restrains the reach of the advancing head, resulting in center-of-mass steps of 8 nm (Figure S16A). However, the two motor rings might occasionally separate into an extended conformation that permits a greater reach of the leading head and a consequently larger step size. Much of the step size variation can be explained by the trailing head passing the leading head and landing on various possible binding sites, although ~4 nm steps might be best explained by an inchworm-like progression (Hua et al., 2002) in which the heads do not pass one another (see Figure S16 for models of differently sized stepping). The notion of extended and compact states of the dynein dimer also is suggested by our structure-function studies, which show that a truncation (GST-Dyn1<sub>314kDa</sub>) that reduces the spacing between the two dynein motor domains results in fewer large steps and that insertion of an artificial linker (two  $\alpha$ -actinin repeats) after this truncation point partially restores large steps (Figure 6).

Large forward-backward stepping also may be explained by a compact to extended conformational change in the dynein dimer induced by load (Figure 6A). Increased strain on the leading head (caused by the greater head-to-head separation in the extended state) would then favor its detachment and a backward step. This interpretation is supported by our finding that the probability of taking a backward step increases with the size of the preceding forward step (Figure S11A). Our finding of temporally correlated, forward-backward steps of similar sizes (clustering shown in Figures 4 and S6–S11) also raises the possibility of the existence of multiple, discrete extended conformations, which could arise due to different extents of the detachment of the linker element from the dynein ring or the unzipping of the proximal tail.

### ATP-Independent Walking: How Force Might Modulate Dynein-Microtubule Interactions

Unexpectedly, we discovered that dynein moves processively toward either the minus end or plus end of microtubules under the constant force of an optical trap in the absence of ATP hydrolysis. The ATP independence of forced-backward movement of dynein differs from that described for kinesin-1, where backward movement under superstall forces has been shown to be dependent upon ATP (Carter and Cross, 2005). In contrast to kinesin and similar to our findings with dynein, Gebhardt et al. (2006) showed that a superstall force will induce backward stepping of myosin-V in an ATP-independent manner. However, the opposite pull (an assisting load) could not induce myosin-V movement in the absence of ATP, in contrast to what we observe for dynein. Thus, our results show that an applied force can coordinate cycles of binding and release of dynein's motor domains in both directions along the microtubule in the absence of nucleotide-derived energy.

Our preferred model for dynein's mechanical asymmetry is based on direct strain sensing by the MTBD (Figure 7, pathways A and B). Unlike myosin and kinesin where the polymer interface is located on the surface of the ATPase

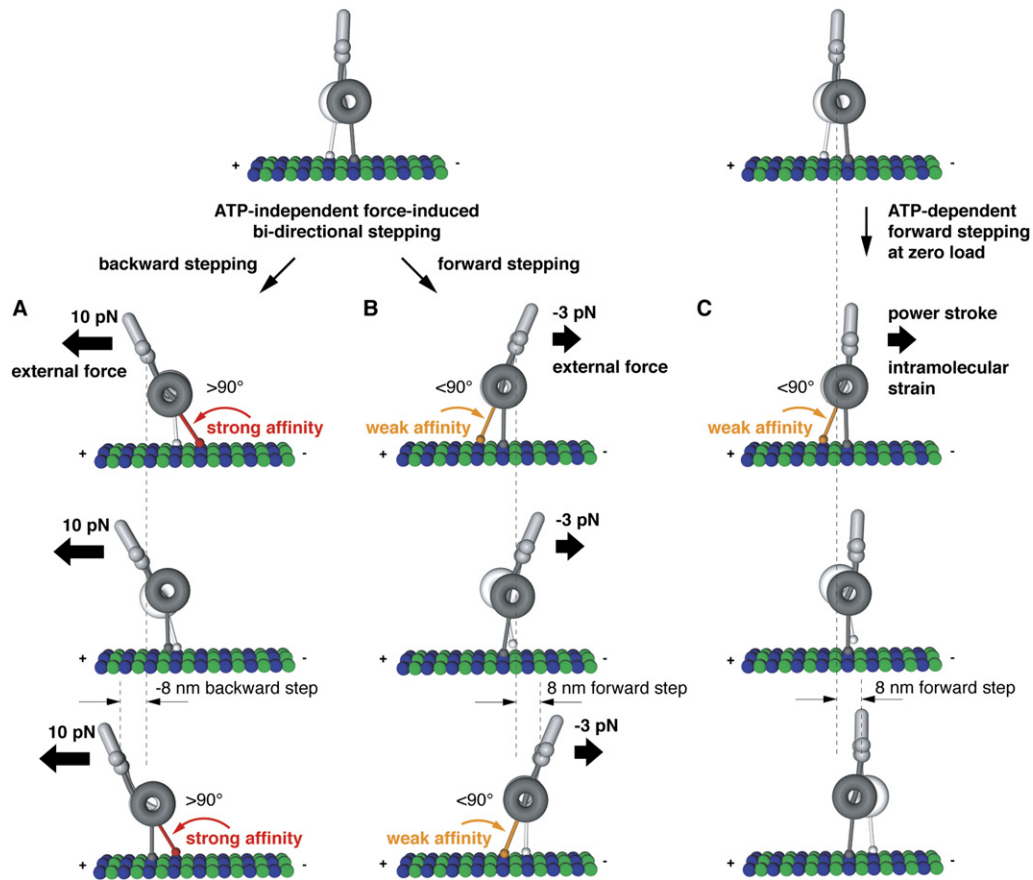


**Figure 7. Model for Force-Induced ATP-Independent Bidirectional Stepping and ATP-Dependent Forward Stepping of Cytoplasmic Dynein**

Mechanical pathways for force-induced backward (A) and forward (B) stepping and an ATP-dependent pathway for normal forward stepping (C). The key feature proposed for these pathways is a tension-sensing mechanism by the MTBD. In these models, forward deflection of the stalk (induced by external forward load [pathway B] or intramolecular strain provided by a power stroke [pathway C]) weakens the binding affinity of the MTBD in the rear head (indicated by the orange-colored stalks). This mechanism favors rear head detachment and thus helps to keep the dynein heads out-of-phase during continuous movement toward the microtubule minus end. Backward load potentially increases the microtubule-binding affinity of the MTBD in the front head (caused by a load-induced backward deflection of the stalk) (indicated by the red-colored stalk), which explains the large external loads required to induce backward stepping. The size of the  $\alpha/\beta$  tubulin dimers and the length of the stalk and the diameter of the dynein ring are drawn to scale. See the Discussion for more details.

core, dynein's MTBD is situated at the end of an  $\sim 10$ – $15$  nm antiparallel coiled-coil stalk (Figure 1A). The stalk is likely to bend or change its angle with an applied load, the exact degree of which will depend upon the geometry of the microtubule-dynein-bead complex and the stiffness of the stalk. We postulate that the detachment rate of the MTBD is sensitive to the stalk angle, with angular displacements toward the microtubule minus end ( $<90^\circ$ , relative to the microtubule) increasing the dissociation rate. Under an external forward load, the stalk angle of the rear head would move closer to  $0^\circ$ , thus favoring rear head dissociation. After detachment, the forward load would shift the dynein molecule toward the microtubule minus end, allowing the detached head to pass its partner head and rebind to an available tubulin-binding site toward the minus end (Figure 7, pathway B). By repetitive

cycles of force-induced rear head detachment, the motor could move toward the minus end in the absence of ATP. In contrast, a rearward load would pull the stalk of the forward head toward  $180^\circ$  (Figure 7, pathway A), a situation that might strengthen its affinity for the microtubule. As this strongly bound front head must detach in order for the motor to step toward the microtubule plus end, this model would explain the higher mechanical load ( $>7$  pN) required to induce plus-end- versus minus-end-directed stepping.

The strain-dependent modulation of the microtubule-binding affinity also might be important for dynein's normal ATP-dependent processive motion (Figure 7, pathway C). In this pathway, we suggest that increased intramolecular strain is induced by an ATP-dependent power stroke in the leading head (reviewed in Spudich, 2006), which

could shift the stalk angle of the trailing head closer to  $0^\circ$  and promote its detachment. Thus, an asymmetric tension-sensing mechanism by the MTBD that favors ATP-dependent (Figures 2C and 5B) rear head detachment could help to keep the dynein heads out-of-phase during processive motion and bias motion toward the microtubule minus end.

### Implication of Dynein's Load-Dependent Stepping and Its Biological Role

The force-dependent properties of cytoplasmic dynein are likely adapted for its biological functions. Yeast cytoplasmic dynein produces a stall force that is comparable to kinesin's (Visscher et al., 1999). However, while kinesin dissociates after a few seconds at stall loads, yeast cytoplasmic dynein frequently remains bound tenaciously to the microtubule for minutes without dissociating. These properties would aid yeast dynein's *in vivo* function in which, most likely, relatively few dyneins pull the large elongating spindle into the daughter cell during cell division.

The ability of yeast dynein to remain microtubule bound and walk backward at superstall forces likely provides new clues for how dynein might operate during spindle positioning and how spindle oscillations might originate (observed along the mother-daughter axis in budding yeast [Yeh et al., 2000] and perpendicular to the anterior-posterior axis of developing *C. elegans* embryos [Pecreaux et al., 2006 and citations therein]). A recent model proposed that spindle oscillations in *C. elegans* embryos are based upon the force-dependent detachment rate of dynein from an astral microtubule (Pecreaux et al., 2006). However, our findings raise another possibility—that dynein could remain attached to an astral microtubule without letting go for several minutes and actively step backward under the opposing forces toward the opposite cell cortex. In addition, dynein's ability to step forward under low assisting force (without detaching or strongly resisting, even under nucleotide-free conditions) would allow “inactive” or “out-of-phase” dynein motors to passively step along the microtubule without strongly interfering with the active motors acting upon the same astral microtubule.

The ability of cytoplasmic dynein to remain microtubule bound and walk backward at superstall forces also makes this motor well suited for a “tug-of-war” with microtubule-plus-end-directed kinesin motor proteins (Gross, 2004; Gennerich and Schild, 2006). Although cytoplasmic dynein does not appear to be involved in organelle transport in yeast, dyneins and kinesins in other eukaryotic organisms appear to be simultaneously bound to various cargos such as organelles, RNP complexes, and chromosomes, generating salutatory bidirectional motion of the cargo (Welte, 2004). At times when kinesin-generated forces exceed those generated by dyneins, dynein could take several steps toward the plus end without letting go of the microtubule; once the opposing force decreases below the stall force level, dynein would immediately be ready to pull again on the microtubule. The low energy

barrier difference for dynein stepping in the forward and backward directions ( $1.3 k_B T$  at zero load; Figure S17) also might be subject to modification by dynein regulatory proteins. In support of such a possibility, Ross et al. (2006) have recently shown that dynein-dynactin complexes can undergo long movements toward the microtubule plus end.

Another setting in which bidirectional dynein movement may occur is in the flagellum. Nanometer-scale, bidirectional oscillations of microtubule sliding have been described in isolated flagella, and it has been postulated that dynein molecules may have an intrinsic tendency to oscillate (Kamimura and Kamiya, 1989, 1992; Shingyoji et al., 1998). Such oscillations may reflect a mechanical feedback cycle that involves load-induced reversal of dynein stepping, as described in this study. During the rapid bending of cilia/flagella, this would allow dyneins on one side of the axoneme to step passively toward the plus end while dyneins on the opposite side are generating minus-end-directed power strokes. Further work will be required to establish whether axonemal dynein (and also cytoplasmic dyneins from other species) show some of the same biophysical properties that we describe here for yeast cytoplasmic dynein and whether such behavior occurs under the loads that these motors experience in living cells.

## EXPERIMENTAL PROCEDURES

### Protein Expression and Purification

Full-length (Dyn<sub>1471kDa</sub>) and truncated artificially dimerized cytoplasmic dynein (GST-Dyn<sub>1314kDa</sub> and GST-Dyn<sub>1331kDa</sub>) from *Saccharomyces cerevisiae* were prepared and purified as described (Reck-Peterson et al., 2006). GST- $\alpha 2$ -Dyn<sub>1314kDa</sub> was constructed from GST-Dyn<sub>1314kDa</sub> by inserting a DNA fragment encoding residues Q760 to D1002 from the myosin motor- $\alpha$ -actinin fusion construct reported by Kliche et al. (PDB 1G8XI; Kliche et al., 2001). The codon usage was optimized for expression in *S. cerevisiae* and the fragment synthesized by Bio Basic Inc. (Markham, Ontario, Canada). All constructs contained an N-terminal IgG-binding domain and TEV protease cleavage site for protein purification and a terminal GFP for the coupling to anti-GFP antibody-coated latex beads. Before use, all dynein constructs were purified by microtubule affinity (Reck-Peterson et al., 2006).

### Optical Trapping Assay

Experiments were performed with a custom-built force-feedback enhanced optical trapping microscope (Supplemental Experimental Procedures). In brief, bead displacement was detected by a quadrant photodiode and recorded at 2 kHz. Carboxylated latex beads (0.92  $\mu\text{m}$  diameter; Invitrogen) were sparsely covered with the GFP-tagged motor proteins via affinity-purified anti-GFP antibodies. The assay solution consisted of 30 mM HEPES (pH 7.2), 2 mM MgAcetate, 1 mM EGTA, 1 mM MgATP, 1 mg/ml casein, 10 mM DTT, 4.5 mg/ml glucose, and an oxygen scavenger system (Supplemental Experimental Procedures). Measurements in the absence of ATP were performed in the same buffer without supplemental ATP in the presence of 10 U/ml apyrase to remove both residual ATP and ADP. Nucleotide-free measurements were undertaken in a specialized  $\sim 40 \mu\text{l}$  flow cell to permit a buffer exchange. Bead displacement did not occur under these conditions unless a mechanical load was applied confirming ATP depletion. After the completion of the force-clamp measurements in the

absence of nucleotides, the buffer solution was exchanged by a solution containing dynein-coated beads and 1 mM supplemental ATP to verify the axoneme polarity by minus-end-directed bead movement. Motor steps (approximate center-of-mass movement of dynein) were determined from the bead displacement records using a step-finding algorithm developed by Kerssemakers et al. (2006), and the details of this analysis are described in the [Supplemental Experimental Procedures](#).

### Supplemental Data

Supplemental Data include Supplemental Experimental Procedures and eighteen figures and can be found with this article online at <http://www.cell.com/cgi/content/full/131/5/952/DC1/>.

### ACKNOWLEDGMENTS

The authors wish to thank A. Yildiz, T. Purcell, D. Lörke, O. Akin, E. Lemke, and K. Slep for stimulating discussions; J. Kull for structural advice; J. Kerssemakers and M. Dogterom for generously providing their step-finding program ahead of publication; and T. Purcell for generously providing a Matlab script for generating artificial optical trapping-based motor traces. This work has been supported by the Jane Coffin Childs Foundation (A.G. and A.P.C.), the German Research Foundation (GE 1609/1 [A.G.]), the National Institutes of Health (P01-AR42895 [R.D.V.] and F32-GM67403-02 [S.R.-P.]), the Agouron Institute (A.P.C.), the Leukemia and Lymphoma Society (A.P.C.), and the Howard Hughes Medical Institute.

Received: April 3, 2007

Revised: July 24, 2007

Accepted: October 8, 2007

Published: November 29, 2007

### REFERENCES

- Asai, D.J., and Koonce, M.P. (2001). The dynein heavy chain: structure, mechanics and evolution. *Trends Cell Biol.* *11*, 196–202.
- Bell, G.I. (1978). Models for the specific adhesion of cells to cells. *Science* *200*, 618–627.
- Burgess, S.A., Walker, M.L., Sakakibara, H., Knight, P.J., and Oiwa, K. (2003). Dynein structure and power stroke. *Nature* *421*, 715–718.
- Carter, N.J., and Cross, R.A. (2005). Mechanics of the kinesin step. *Nature* *435*, 308–312.
- Gebhardt, J.C., Clemen, A.E., Jaud, J., and Rief, M. (2006). Myosin-V is a mechanical ratchet. *Proc. Natl. Acad. Sci. USA* *103*, 8680–8685.
- Gee, M.A., Heuser, J.E., and Vallee, R.B. (1997). An extended microtubule-binding structure within the dynein motor domain. *Nature* *390*, 636–639.
- Gennerich, A., and Schild, D. (2006). Finite-particle tracking reveals submicroscopic-size changes of mitochondria during transport in mitral cell dendrites. *Phys. Biol.* *3*, 45–53.
- Gross, S.P. (2004). Hither and yon: a review of bi-directional microtubule-based transport. *Phys. Biol.* *1*, R1–R11.
- Höök, P., and Vallee, R.B. (2006). The dynein family at a glance. *J. Cell Sci.* *119*, 4369–4371.
- Hua, W., Chung, J., and Gelles, J. (2002). Distinguishing inchworm and hand-over-hand processive kinesin movement by neck rotation measurements. *Science* *295*, 844–848.
- Kamimura, S., and Kamiya, R. (1989). High-frequency nanometre-scale vibration in ‘quiescent’ flagellar axonemes. *Nature* *340*, 476–478.
- Kamimura, S., and Kamiya, R. (1992). High-frequency vibration in flagellar axonemes with amplitudes reflecting the size of tubulin. *J. Cell Biol.* *116*, 1443–1454.
- Kerssemakers, J.W., Munteanu, E.L., Laan, L., Noetzel, T.L., Janson, M.E., and Dogterom, M. (2006). Assembly dynamics of microtubules at molecular resolution. *Nature* *442*, 709–712.
- King, S.J., and Schroer, T.A. (2000). Dynactin increases the processivity of the cytoplasmic dynein motor. *Nat. Cell Biol.* *2*, 20–24.
- Kliche, W., Fujita-Becker, S., Kollmar, M., Manstein, D.J., and Kull, F.J. (2001). Structure of a genetically engineered molecular motor. *EMBO J.* *20*, 40–46.
- Kon, T., Nishiura, M., Ohkura, R., Toyoshima, Y.Y., and Sutoh, K. (2004). Distinct functions of nucleotide-binding/hydrolysis sites in the four AAA modules of cytoplasmic dynein. *Biochemistry* *43*, 11266–11274.
- Kon, T., Mogami, T., Ohkura, R., Nishiura, M., and Sutoh, K. (2005). ATP hydrolysis cycle-dependent tail motions in cytoplasmic dynein. *Nat. Struct. Mol. Biol.* *12*, 513–519.
- Koonce, M.P., and Tikhonenko, I. (2000). Functional elements within the dynein microtubule-binding domain. *Mol. Biol. Cell* *11*, 523–529.
- Mallik, R., Carter, B.C., Lex, S.A., King, S.J., and Gross, S.P. (2004). Cytoplasmic dynein functions as a gear in response to load. *Nature* *427*, 649–652.
- Mallik, R., Petrov, D., Lex, S.A., King, S.J., and Gross, S.P. (2005). Building complexity: an in vitro study of cytoplasmic dynein with in vivo implications. *Curr. Biol.* *23*, 2075–2085.
- Mehta, A.D., Rock, R.S., Rief, M., Spudich, J.A., Mooseker, M.S., and Cheney, R.E. (1999). Myosin-V is a processive actin-based motor. *Nature* *400*, 590–593.
- Nishikawa, S., Homma, K., Komori, Y., Iwaki, M., Wazawa, T., Hiki-koshi Iwane, A., Saito, J., Ikebe, R., Katayama, E., Yanagida, T., and Ikebe, M. (2002). Class VI myosin moves processively along actin filaments backward with large steps. *Biochem. Biophys. Res. Commun.* *290*, 311–317.
- Ogura, T., and Wilkinson, A.J. (2001). AAA+ superfamily of ATPases: common structure - diverse function. *Genes Cells* *6*, 575–597.
- Pecreaux, J., Röper, J.C., Kruse, K., Jülicher, F., Hyman, A.A., Grill, S.W., and Howard, J. (2006). Spindle oscillations during asymmetric cell division require a threshold number of active cortical force generators. *Curr. Biol.* *16*, 2111–2122.
- Reck-Peterson, S.L., and Vale, R.D. (2004). Molecular dissection of the roles of nucleotide binding and hydrolysis in dynein’s AAA domains in *Saccharomyces cerevisiae*. *Proc. Natl. Acad. Sci. USA* *101*, 1491–1495.
- Reck-Peterson, S.L., Yildiz, Y., Carter, A.P., Gennerich, A., Zhang, N., and Vale, R.D. (2006). Single molecule analysis of dynein processivity and stepping behavior. *Cell* *126*, 335–348.
- Rock, R.S., Rice, S.E., Wells, A.L., Purcell, T.J., Spudich, J.A., and Sweeney, H.L. (2001). Myosin VI is a processive motor with a large step size. *Proc. Natl. Acad. Sci. USA* *98*, 13655–13659.
- Ross, J.L., Wallace, K., Shuman, H., Goldman, Y.E., and Holzbaur, E.L. (2006). Processive bidirectional motion of dynein-dynactin complexes in vitro. *Nat. Cell Biol.* *8*, 562–570.
- Shingyoji, C., Higuchi, H., Yoshimura, M., Katayama, E., and Yanagida, T. (1998). Dynein arms are oscillating force generators. *Nature* *393*, 711–714.
- Silvanovich, A., Li, M.G., Serr, M., Mische, S., and Hays, T.S. (2003). The third P-loop domain in cytoplasmic dynein heavy chain is essential for dynein motor function and ATP-sensitive microtubule binding. *Mol. Biol. Cell* *14*, 1355–1365.
- Spudich, J.A. (2006). Molecular motors take tension in stride. *Cell* *126*, 242–244.
- Svoboda, K., Schmidt, C.F., Schnapp, B.J., and Block, S.M. (1993). Direct observation of kinesin stepping by optical trapping interferometry. *Nature* *365*, 721–727.

- Takahashi, Y., Edamatsu, M., and Toyoshima, Y.Y. (2004). Multiple ATP-hydrolyzing sites that potentially function in cytoplasmic dynein. *Proc. Natl. Acad. Sci. USA* *101*, 12865–12869.
- Toba, S., Watanabe, T.M., Yamaguchi-Okimoto, L., Toyoshima, Y.Y., and Higuchi, H. (2006). Overlapping hand-over-hand mechanism of single molecular motility of cytoplasmic dynein. *Proc. Natl. Acad. Sci. USA* *103*, 5741–5745.
- Vale, R.D. (2003). The Molecular motor toolbox for intracellular transport. *Cell* *112*, 467–480.
- Vallee, R.B., Williams, J.C., Varma, D., and Barnhart, L.E. (2004). Dynein: An ancient motor protein involved in multiple modes of transport. *J. Neurobiol.* *58*, 189–200.
- Veigel, C., Wang, F., Bartoo, M.L., Sellers, J.R., and Molloy, J.E. (2002). The gated gait of the processive molecular motor, myosin V. *Nat. Cell Biol.* *4*, 59–65.
- Visscher, K., Schnitzer, M.J., and Block, S.M. (1999). Single kinesin molecules studied with a molecular force clamp. *Nature* *400*, 184–189.
- Walker, M.L., Burgess, S.A., Sellers, J.R., Wang, F., Hammer, J.A., 3rd, Trinick, J., and Knight, P.J. (2000). Two-headed binding of a processive myosin to F-actin. *Nature* *405*, 804–807.
- Wang, Z., Khan, S., and Sheetz, M.P. (1995). Single cytoplasmic dynein molecule movements: Characterization and comparison with kinesin. *Biophys. J.* *69*, 2011–2023.
- Welte, M.A. (2004). Bidirectional transport along microtubules. *Curr. Biol.* *14*, R525–R537.
- Yeh, E., Yang, C., Chin, E., Maddox, P., Salmon, E.D., Lew, D.J., and Bloom, K. (2000). Dynamic positioning of mitotic spindles in yeast: role of microtubule motors and cortical determinants. *Mol. Biol. Cell* *11*, 3949–3961.